

## The magnitude and impact of the 431 CE Tierra Blanca Joven eruption of Ilopango, El Salvador

Victoria C. Smith<sup>1\*</sup>, Antonio Costa<sup>2\*</sup>, Gerardo Aguirre-Díaz<sup>3</sup>, Dario Pedrazzi<sup>4</sup>, Andrea Scifo<sup>5</sup>, Gill Plunkett<sup>6</sup>, Mattieu Poret<sup>7</sup>, Pierre-Yves Tournigand<sup>8</sup>, Dan Miles<sup>1</sup>, Michael W. Dee<sup>5</sup>, Joseph R. McConnell<sup>9</sup>, Ivan Sunyé-Puchol<sup>3,1</sup>, Pablo Dávila Harris<sup>10</sup>, Michael Sigl<sup>11</sup>, Jonathan R. Pilcher<sup>6</sup>, Nathan Chellman<sup>9</sup>, Eduardo Gutiérrez<sup>12</sup>

1. Research Laboratory for Archaeology and the History of Art, School of Archaeology, University of Oxford, Oxford OX1 3TG, UK. [\\*victoria.smith@arch.ox.ac.uk](mailto:victoria.smith@arch.ox.ac.uk) <https://orcid.org/0000-0003-0878-5060>
2. Istituto Nazionale di Geofisica e Vulcanologia, Bologna 40128, Italy. [\\*antonio.costa@ingv.it](mailto:antonio.costa@ingv.it) <https://orcid.org/0000-0002-4987-6471>
3. Centro de Geociencias, Universidad Nacional Autónoma de México, Querétaro 76230, Mexico.
4. Group of Volcanology, Laboratory of Geological Processes Simulation (SIMGEO UB-CSIC), Institute of Earth Sciences Jaume Almera, Lluís Sole i Sabarís s/n, 08028 Barcelona, Spain
5. Centre for Isotope Research, University of Groningen, Groningen 9747 AG, the Netherlands.
6. Archaeology & Palaeoecology, School of Natural and Built Environment, Queen's University Belfast, Belfast BT7 1NN, Northern Ireland, UK
7. Laboratoire Magmas et Volcans, Université Clermont Auvergne, CNRS, Institut de Recherche pour le Développement, 63170 Clermont-Ferrand, France.
8. Dipartimento di Geoscienze, Università degli studi di Padova, 35131 Padua, Italy
9. Desert Research Institute, Reno, Nevada 89512, USA
10. División de Geociencias Aplicadas, Instituto Potosino de Investigación Científica y Tecnológica, San Luis Potosí 78216, Mexico.
11. Climate and Environmental Physics, Physics & Oeschger Centre for Climate Change Research, University of Bern, Sidlerstrasse 5, 3012 Bern, Switzerland
12. Gerencia de Geología del Observatorio Ambiental, Ministerio de Medio Ambiente y Recursos Naturales, San Salvador 76230, El Salvador

### Corresponding authors:

[victoria.smith@arch.ox.ac.uk](mailto:victoria.smith@arch.ox.ac.uk); [antonio.costa@ingv.it](mailto:antonio.costa@ingv.it)

PDF includes:

Main text: ~5248 words and 59 references

4 Figures

2 Tables

Supporting Information

### Classification

Physical Sciences; Earth, Atmospheric, and Planetary Sciences

### Keywords

Maya; large volcanic eruptions; sulfate; eruption dispersal; ice cores; radiocarbon

## **Abstract**

The Tierra Blanca Joven (TBJ) eruption from Ilopango volcano deposited thick ash over much of El Salvador when it was inhabited by the Maya, and rendered all areas within at least 80 km of the volcano uninhabitable for years to decades after the eruption. Nonetheless the more widespread environmental and climatic impacts of this large eruption are not well known because the eruption magnitude and date are not well constrained. In this multifaceted study we have: resolved the date of the eruption to  $431 \pm 2$  CE by identifying the ash layer in a well dated, high-resolution Greenland ice core record that is  $>7,000$  km from Ilopango; and calculated that between 37 and 82 km<sup>3</sup> of magma was dispersed from an eruption coignimbrite column that rose to  $\sim 45$  km by modeling the deposit thickness using state-of-the-art tephra dispersal methods. Sulfate records from an array of ice cores suggest stratospheric injection of  $14 \pm 2$  TgS associated with the TBJ eruption, exceeding those of the historic eruption of Pinatubo in 1991. Based on these estimates it is likely that the TBJ eruption produced a cooling of around 0.5°C for a few years after the eruption. The modeled dispersal and higher sulfate concentrations recorded in Antarctic ice cores imply that the cooling would have been more pronounced in the Southern Hemisphere. The new date confirms the eruption occurred within the Early Classic phase when Maya expanded across the Central America.

## **Significance statement**

The TBJ eruption of Ilopango occurred during Maya times but the exact timing and its impact have been controversial. It was thought to be responsible for the anomalously cold decade experienced in the Northern Hemisphere centered at 540 CE, but this date is at odds with archeological evidence that suggests a date near the start of the Early Classic period (pre-450 CE). Our precise age of  $431 \pm 2$  CE allows us to pinpoint the eruption in proxy records and shows that its impact was apparently limited. It appears to have only had major effects on populations within  $\sim 80$  km of the volcano, where the regions were blanketed by decimeters of ash fallout and pyroclastic density currents.

## **Introduction**

There have only been two large magnitude volcanic eruptions in the last two hundred years (erupted  $>10$  km<sup>3</sup> of magma;  $VEI \geq 6$ ) (1) for which we have well documented records of the impact. Like wildfires, tropical cyclones, tsunamis, and earthquakes, volcanic eruptions result in catastrophic local to regional impacts. However, one thing that sets eruptions apart from other natural hazards is the potential for more widespread effects associated with the injection of aerosols, especially sulfate, into the upper atmosphere. Sulfate aerosols that reach the stratosphere increase albedo and result in decreases in temperature at the Earth's surface on the hemispheric to global scale (2). After the 1991 Pinatubo (Philippines) eruption there was decline of up to 1°C in the sub-tropical troposphere (3) and following the 1815 CE eruption of Tambora (Indonesia), cooler summers were experienced in North America and Europe. These cooler temperatures in 1816–1818 CE resulted in reduced growing seasons and poor harvests, which led to famine and high mortality across Europe and North America (4, 5). The impact of these eruptions is clear as they are comparatively recent and well documented, but evaluating the impact of similarly large eruptions further back in time is more difficult as written accounts often do not exist and there are large uncertainties in calculating the magnitude of the eruption and the amount of sulfate aerosols released. One way to establish the impact on climate and society is to use paleoenvironmental and archeological records, but this relies on identifying the

eruption deposits within them, or obtaining a precise date for the eruption, so it can be pinpointed in records to evaluate its timing relative to climate and cultural changes.

Large regions of El Salvador and its Maya sites were covered by thick deposits from an eruption that occurred during the Early Classic Period that lasted from 300 to 600 CE (6-8). The eruption that generated these deposits is named the Tierra Blanca Joven (TBJ) after its prominent outcrops of “young white earth”. The eruption occurred from the Ilopango caldera, a 13 by 17 km collapse structure, formed and modified by its numerous large eruptions in the last 1.8 Ma (9, 10). The thickness of the deposits around the vent testifies to a large magnitude event, and such eruptions release sulfur into the stratosphere that converts into sulfate. This stratospheric sulfate gradually falls out, forming a deposit that can be detected in the polar ice cores (11, 12). In 540 CE, there are a couple of large non-sea salt sulfur (nssS) peaks in ice core records retrieved from both polar ice-sheets, which are consistent with a tropical eruption that injected volatiles into both hemispheres (13). Given that this falls within the range of radiocarbon dates for the TBJ eruption (270-562 CE; 95.4% probability), the date of the eruption was pinpointed to the ice core nssS spike at 540 CE (14). However, the published radiocarbon measurements (quoted above) are poorly constrained as they correspond with a plateau in the radiocarbon calibration curve and there are other earlier nssS peaks that could have been generated by the TBJ eruption. The suggestion that the eruption occurred at 540 CE (14) is controversial as archeologists working in the region have recovered artefacts in Chalchuapa, 75 km NNW of Ilopango (Fig. 1) that were clearly influenced by Teotihuacan Culture from beneath the TBJ ash in the Tazumal and Casa Blanca archeological sites. These Teotihuacan items are typical of those made at the start of the Early Classic Period (7) and hence, imply the eruption occurred prior to 450 CE. Furthermore, Maya ceramic assemblages recovered from archeological sites in El Salvador are similar to those found elsewhere in the region, but after about 400 CE it appears that ceramic production ceased in El Salvador for a period of around 100–150 years (15).

We examined both the regional and more widespread impact of the TBJ eruption via a multifaceted study. We have brought together a range of methods to assess the magnitude of the eruption and height of the eruption plumes. To pinpoint the eruption in paleoenvironmental records we also reassessed the date of the eruption by wiggle-matching radiocarbon measurements of successive tree rings onto the radiocarbon calibration curve. This improved date then provided constraints for us refine its date using a high-resolution polar ice core and its precise chronology (16). Our date also allows us to define the timing of the eruption within cultural and climate records, which can be used to assess how this eruption affected the region.

### **The Tierra Blanca Joven eruption**

The TBJ deposits provide evidence that the eruption produced eruption plumes and fueled numerous pyroclastic density currents (PDCs) (17, 18). The first two eruptive phases were predominantly magmatic fallout with minor hydromagmatic activity. These were followed by a sequence of PDC units (19), which deposited dense to dilute currents. These deposits extend 50 km from the vent (Fig. 1) and are up to 70 m thick in valleys near the caldera. Pedrazzi et al. (19) estimated the volume of the PDC deposits to be at least 13 km<sup>3</sup> dense rock equivalent (DRE). The PDCs generated a high coignimbrite (co-PDC) phoenix plume that caused widespread dispersal of the volcanic ash over Guatemala, Honduras, Nicaragua, Costa Rica, and the Pacific Ocean (19).

### **Magnitude and dispersal of the TBJ eruption**

The deposit thicknesses at more than 72 locations (data from ref. 19 and 20; see Methods) were used to produce a 3D numerical model (FALL3D) (21) reconstructing tephra dispersal from the coignimbrite phase and estimating the associated eruption parameters following the method proposed by Costa et al. (22, 23). This 3D approach uses: a set of time-dependent meteorological fields from across the region, which were obtained from the European Centre for Medium-Range Weather Forecasts global atmospheric reanalysis (ERA-Interim); a range of volcanological input parameters that include total erupted mass, mass eruption rate, column height, and total grain size distribution; and several hundred simulations of the FALL3D tephra dispersal model (21, 24). Further details of the modeling inversion and the use of the input parameters in FALL3D are detailed in recent studies (25). The range of volcanological input parameters used within the models were based on those estimated in the analytical model of Pedrazzi et al. (19) for the TBJ deposits. The FALL3D code is based on the numerical solution of a set of advection-diffusion-sedimentation equations coupled to a model that describes the density-driven transport responsible for the radial growth of the volcanic cloud at the neutral buoyancy level (24). The optimal eruption parameter values are obtained by producing best fits to measured TBJ deposit thicknesses across the dispersal area (shown in Fig. 1). These simulated results are in general agreement with the measured thicknesses, with most of the simulated thicknesses between 1/5 and 5 times those observed (see *SI Appendix*, Fig. S1).

The FALL3D model results indicate approximately 55 km<sup>3</sup> DRE was dispersed from the turbulent coignimbrite plume that rose to a height of 45 km, with approximately 34 km<sup>3</sup> DRE of material released into the stratosphere. The mean error associated with the estimation of the erupted mass is about a factor 1.5, which indicates that the volume of magma dispersed by the plume was between 37 and 82 km<sup>3</sup> DRE, and the maximum error is a factor 3. The fallout associated with this enormous and unstable plume covered approximately 2 million km<sup>2</sup> with  $\geq 0.5$  cm of ash within a few days (see *SI Appendix*, SIM1 movie). Adding the volumes of the PDCs (13 km<sup>3</sup>) (19) takes the total volume of magma erupted during the TBJ eruption to between 50 and 95 km<sup>3</sup> DRE.

### **Radiocarbon measurements and Bayesian age modeling**

To determine the date of the eruption we looked for organic material within the TBJ deposits. A slightly charred tree was found in late PDC deposits of the TBJ eruption at a location around 25 km NNW from Ilopango. The bark of the Mahogany tree (family Meliaceae) stump was intact and a cross section through the stump revealed  $\leq 37$  growth rings. Samples for radiocarbon dating were taken from packets of these rings, representing approximately 10 years, along two sections that extended out from the pith to the bark edge of the stump. The radiocarbon measurements of these samples were performed using a state-of-the-art Micadas Accelerator Mass Spectrometer at the University of Groningen. These precise <sup>14</sup>C measurements were wiggle-matched onto the IntCal13 calibration curve (26) using a Bayesian statistical model (*D\_Sequence* in OxCal) (27) to establish the date on which the tree was incorporated into the TBJ PDC (Table 1). The bark edge dates from each section were then merged in a separate OxCal model (*Combine* function), and indicate the TBJ eruption occurred between 425 and 440 CE (95.4% probability; Fig. 2). This is a significant improvement on previous radiocarbon determinations for the eruption, which span from 270 to 562 CE (95.4% probability).

Radiocarbon dates from other trees in the TBJ deposits were recently published (14) and include cross-sections from three tree stumps that were similarly modeled onto a radiocarbon

calibration curve using Bayesian statistics. However, the authors used a mixed radiocarbon calibration curve, which combines the Southern Hemisphere SHCal13 (29) and Northern Hemisphere IntCal13 (26) datasets, to calibrate the radiocarbon measurements and obtained calendar dates of 435-562 CE (95.4% probability) for two of the stumps. Their third stump (El Mico A) produced an older age that sits just outside the range of the other two and because it was particularly decomposed, they suggest that it was dead prior to being incorporated into the flow (14). The justification for using a mixed calibration, 69% Northern Hemisphere and 31% Southern Hemisphere, curve was the tropical location of these trees (14), but Ilopango is at 13.8 °N and clearly sits within a main Northern Hemisphere  $^{14}\text{C}$  zone (30). Furthermore, recent studies suggest air masses over El Salvador come from Northern Hemisphere in both the austral summer and winter (31), which is also shown by the TBJ dispersal (Fig. 1). If the Dull et al. (14) data are calibrated using the accepted IntCal13 curve, the range of dates is slightly older than those reported in their paper, with one mode at 401-431 CE and another at 471-530 CE (95.4% probability; *SI Appendix*, Fig. S3-S5). The older age range is consistent with our new radiocarbon data.

### **Identifying the TBJ in the polar ice cores**

Within the timeframe established by the wiggle-match radiocarbon date (425-440 CE; 95.4% probability) there is an apparently contemporaneous nssS spike in various Antarctic and Greenland ice cores (Fig. 3). Continuous measurements of the TUNU2013 ice core from northeast Greenland reveal an increase in particles at 431 CE (depth of 194.395 to 194.48 m on the master age-depth scale; Fig. 3) followed by a spike in nssS of up to ~90 ppb ( $\mu\text{g/g}$ ) at 433 CE. Absolute age uncertainties at this depth are estimated to be better than  $\pm 2$  years (13, 33). The offset in particle and nssS deposition is consistent with what is observed and modeled for volcanic eruptions, as it takes some time before the nssS is removed from the stratosphere (32, 34). For example, nssS was deposited a few months to a couple of years after the 1815 CE Tambora eruption (35).

Approximately 14-15 volcanic glass shards were identified in the particle-rich TUNU2013 ice sample at 431 CE. Some of these shards had areas that were large enough to be analyzed. The major element compositions of these glass shards entirely overlap with those of the TBJ (Fig. 4; Table 2), and one of the ice core glass shards plots with the less evolved melt erupted during the TBJ eruption, confirming that these shards are distal TBJ ash that travelled 7,750 km. It is not unusual for tephra to travel such distances (23) as other tephra layers identified in Greenland have been correlated to sources up to 8,000 km away (36, 37). This correlation provides additional confidence that the age of the TBJ eruption is  $431 \pm 2$  CE.

## **DISCUSSION**

### **Climatic and environmental impact of the eruption**

Multiple annually dated ice-core chronologies suggest that the large nssS spikes at around 433 CE in the Antarctic and Greenland ice cores are contemporaneous (13, 38). The TBJ glass shards in Greenland confirm that the nssS peak is associated with the TBJ eruption, and although the contemporaneous Antarctic peak could potentially be associated with another volcanic event there are aspects that suggest that is likely to be related to the TBJ eruption. Sulfur isotope measurements on samples encompassing the corresponding 433 CE peak in another ice core from Antarctica show mass independent fractionation ( $\Delta^{33}\text{S} = 0.54 \pm 0.12 \text{ ‰}$ ), which is consistent with sulfate aerosol formation in the stratosphere (39). The broad peak of volcanic sulfur

concentrations, spanning more than 2 years in high-resolution ice-core records from Antarctica (38, 40), is consistent with a distal, low latitude source. Given this evidence and that other large magnitude eruptions from the low latitudes typically deposit sulfur at both poles (38) we consider that the Antarctic nssS peak at 433 CE is associated with the TBJ eruption. Extending tephra analyses to ice-cores from Antarctica could be used to test this attribution in the future. The 433 CE nssS concentrations in ice cores distributed over Greenland are variable, ranging from 40 ppb to 80 ppb, and the highest concentrations recorded in Antarctica are around 60 ppb (Fig. 3). Based on these ice nssS deposits, the TBJ eruption generated one of twenty highest volcanic stratospheric sulfur injections ( $14 \pm 2$  Tg) in the Common Era (33). Analysis of the Common Era ice core dataset shows that large tropical eruptions cause  $0.6 \pm 0.2$  °C cooler temperatures in the northern hemisphere extratropics from June to August for at least four years after the eruption and often do not recover pre-eruption values until 9 years after the eruption (13). More recent work has, however, suggested that the apparent decadal persistency in the reconstructed cooling may be biased from a biological memory in the tree-ring widths data included in the temperature reconstructions (41, 42). The 433 CE ice-core records indicate an asymmetric stratospheric sulfur burden favoring the Southern Hemisphere (Fig. 3) (13). The hemispheric partitioning of sulfate aerosols following tropical eruptions depends on a variety of parameters, most notably the Quasi-biennial oscillation that displays considerable seasonal variation (43, 44). Large low latitude eruptions (e.g., Samalas 1257 CE and Krakatoa 1883 CE) that dispersed more sulfur in the opposing hemisphere (33) highlight that sulfur transport is dependent on the atmospheric circulation. Since the sulfur associated with the TBJ eruption was predominately dispersed into the Southern Hemisphere it is likely the cooling would have been significantly stronger there, with 0.5-1 °C cooler seasons for a few years after the eruption. Unfortunately, there are too few well-dated paleoclimate proxy records for the Southern Hemisphere to verify the climatic effect of the eruption (45).

It is difficult to establish the scale and the duration of the climate change around Ilopango and Central American regions following the eruption as few climate records have been sampled at sufficiently high resolution across this interval (46), with the sensitive proxies only typically being analyzed at intervals spanning 20 years (47). A regional  $\delta^{18}\text{O}$  record of a speleothem shows that rainfall in Central America has been particularly variable over the preceding millennia. It indicates that a period of relatively high rainfall started around 440 CE (7 and references therein) and extended for 50-60 years, much longer than expected if it was purely volcanically-forced. Furthermore, the wet period is similar in magnitude and duration to others in the record that do not coincide with large volcanic events. In summary, data from proxy records in the region do not reveal any pronounced or long-term climate perturbation around the time of the eruption. However, it is possible that there was significant short-term change that has not yet been deciphered in these past environmental records as they have not been analyzed at a sub-decadal resolution.

The input of the TBJ ash into the Pacific Ocean would have altered the ocean chemistry and affected the biogeochemical cycle, especially because the region of the Pacific Ocean south of El Salvador is particularly low in iron and chlorophyll (48). The TBJ ash has similar iron contents ( $\sim 1$  wt% FeO; Table 2) to ash erupted by Pinatubo (Philippines) in 1991 (49) and similarly, Pinatubo deposited ash into a Fe-limited region of the ocean. This additional iron increased marine productivity resulting in  $\text{CO}_2$ -drawdown and a pulse in atmospheric oxygen (50). Given that the TBJ eruption was an order of magnitude greater (total volume 50-95  $\text{km}^3$  DRE) than the Pinatubo

eruption (3-5 km<sup>3</sup> DRE) it would have generated a more pronounced increase in marine productivity and resulted in changes in both atmospheric CO<sub>2</sub> and oxygen in the years following the TBJ eruption.

The dispersal of tephra and distribution of the PDC deposits indicates that areas within 80 km of the vent were covered with decimeters of ash. Everything within these regions would have been destroyed and vegetation would have taken many years to decades to recover (23, 51). Further afield, in the Maya lowlands located more than 450 km from Ilopango where only millimeters of ash would have been deposited, the effects appear to have been limited in this tropical environment, with archeological records suggesting that at the time the number of Maya monuments were increasing along with the population (7).

## Conclusions

The coignimbrite plume generated by the VEI6, Magnitude 6.9-7.3 TBJ eruption from Ilopango volcano dispersed between 85 and 188 km<sup>3</sup> of tephra (37-82 km<sup>3</sup> DRE) over large areas of central America, with the very finest fraction travelling >7,000 km to Greenland. Compositionally identifying the tephra in the ice core provides the precise date of 431 ± 2 CE for the eruption. This conclusive date is earlier than some other studies have suggested (14) but is consistent with all published data from the region. The position of the tephra in the Greenland ice core is associated with a slightly later peak in nssS, and a broad nssS peak linked to a low latitude eruption is observed at the same time in Antarctic ice cores. The coincident spikes in nssS suggest that this tropical eruption injected ~14 Tg of sulfur into the stratosphere which subsequently dispersed in both hemispheres. This injection into the upper atmosphere occurred during the later phases of the eruption when the particularly turbulent and unstable coignimbrite plume extended to a height of 45 km. The local to regional impacts appear to have been restricted to areas within a few hundred kilometers of the vent, with no compelling evidence in paleoenvironmental records or historical accounts for significant impact at this time.

## Methods

**Ash dispersal modeling:** Ash dispersal associated with the TBJ tephra deposits was simulated using the FALL3D model, which solves equations for advection, diffusion and sedimentation of particles (21) and accounts for gravity spreading of the umbrella region (24). The isopach maps were generated by modeling the tephra deposition in terms of mass loading (kg/m<sup>2</sup>) and converting to thicknesses, using a bulk density of 1,000 kg/m<sup>3</sup>, following an approach that has been used for other eruption deposits (22, 23). The thickness measurements used in the FALL3D model are those from Pedrazzi et al., (19), and we included an additional two points where 3 cm of ash was recorded in cores: OC001 at 92.164417°W, 14.539192°N, and MES001 at 92.136236°W, 14.477268°N (20).

The input parameters required for the dispersal model include: mass eruption rate, eruption duration, eruption column height, mass distribution along the column, total grain-size distribution, and meteorological fields across the computational domain. As there is no direct way to estimate all these parameters at the time of the eruption, they were estimated by the model by minimizing the difference between observed and modeled thickness (23, 52):

$$K = \exp \left[ \frac{1}{N} \sum_i^N \log \left( \frac{T_{i(obs)}}{T_{i(calc)}} \right) \right]; \quad k = \exp \left[ \sqrt{\frac{1}{N} \sum_i^N \log \left( \frac{T_{i(obs)}}{T_{i(calc)}} \right)^2} - \left( \frac{1}{N} \sum_i^N \log \left( \frac{T_{i(obs)}}{T_{i(calc)}} \right) \right)^2 \right] \quad (S.1)$$

where  $N$  is the number of data points (sample localities),  $T_i(obs)$  and  $T_i(calc)$  represent the observed and calculated thicknesses, respectively, and  $K$  and  $k$  are the statistical indexes (i.e. geometric average of the distribution and geometric standard deviation of the distribution) introduced by Aida (53).

The model assumes ash was injected into the atmosphere from vertically distributed point sources above the caldera. The TGSD of the coignimbrite deposits (19) was used for the simulations. The model accounts for the aggregation of fine ash using a parameterization (54), which assumes 50% of the 63–44  $\mu\text{m}$  ash, 75% of the 44–31  $\mu\text{m}$  ash, and 95% of the ash <31  $\mu\text{m}$  fell as aggregated particles with an effective diameter of 200  $\mu\text{m}$  (55). The effective density of these aggregates was found to be very low (45  $\text{kg}/\text{m}^3$ ) (19). The other parameters used in the model and the explored ranges are reported in the *SI Appendix*, Table S1. The simulations were carried out using a horizontal resolution of  $\sim 20$  km and a vertical resolution of 2 km.

The reconstruction represents ash dispersal fed by the TBJ coignimbrite plume. However, this best-fit solution is not necessarily unique as there are a wide range of eruption source parameter combinations, the input parameters are inter-dependent, and not all computational settings were fully explored (e.g., 52, 56).

**TUNU2013 ice core chronology:** The 212 m-long TUNU2013 ice core was drilled in 2013 in northeast Greenland (78.04°N, 33.88°W; 2105 m above sea level). The TUNU2013 ice core chronology is based on counts of the annual layers counted between fixed volcanic constraints using non-sea-salt sulfur signals to other Greenland ice cores, with the 774/5 CE cosmogenic event being the nearest calendar-dated fix point (13). This TUNU2013 chronology is within  $\pm 2$  years of the North Greenland Eemian Ice Drilling (NEEM) project (NEEM-2011-S1) ice core timescale (13) and with the independent North Greenland Ice Core (NGRIP) project DRI-NGRIP2 ice-core timescale (57). The particle concentrations and compositional data along the core were determined by analyzing a stream of water obtained by continuously melting a 33×33 mm cross section of the ice (58). The particles in the section where there were elevated concentrations, at 431 CE, were retrieved from the meltwater sample that spans approximately 2.5 years.

**TUNU2013 glass compositions:** Major element geochemical compositions of tephra shards (sample QUB-1983) in the TUNU2013 ice core at 431 CE were determined using a JEOL 6500F field emission gun scanning electron microscope at Queen's University Belfast. An accelerating voltage of 15 kV was used and the beam was set to 5 nA and rastered over a 5×5  $\mu\text{m}$  area. The Na, Mg, Mn and Ti were analyzed using a wavelength dispersive spectrometer (WDS), while the Si, Al, Fe, K, Ca and Cl were collected using the energy dispersive spectrometer. The count times on peak for all elements analyzed using WDS was 20s, while Na was collected for 10s (59). Reference glasses run with the glass shards are included in the *SI Appendix*, SID1 dataset.

## Acknowledgments

Fieldwork in El Salvador was funded by a grant awarded to GJAD (CONACYT-CB grant 240447), and we acknowledge logistical support from the following institutions in El Salvador: Ministerio del Medio Ambiente y Recursos Naturales (MARN), Museo Nacional de Arqueología (MUNA), Universidad de El Salvador, and Policía Nacional Civil (PNC). VS and ISP acknowledge funding from a NERC grant (NE/5009035/1). AC acknowledges the Ministero dell'Istruzione dell'Università e



della Ricerca project Ash-RESILIENCE. AS and MD acknowledge funding from the European Research Council (ERC) (ECHOES, grant #714679). MS acknowledges funding from the ERC European Union's Horizon 2020 research and innovation programme (grant #820047). DP acknowledges support from a Juan de la Cierva grant (IJCI-2016-30482). The collection and analysis of the TUNU2013 core was supported by an NSF-PLR grant (#1204176) awarded to JRM. We thank Walter Hernandez (MARN) and Hugo Díaz Chávez (MUNA) for assistance in the field, Stephen Harris (Department of Plant Sciences, University of Oxford) for identifying the species of the tree that we radiocarbon dated, and Ian Cartwright (School of Archaeology, University of Oxford) for photographing the cross section of the tree. The meteorological data (ERA-Interim) were provided by European Center for Medium-Range Weather Forecasts (ECMWF). We thank three anonymous reviewers and the handling editor, Michael Manga, for their detailed reviews and constructive comments.

## References

1. C. G. Newhall, S. Self, The Volcanic Explosivity Index (VEI): an estimate of explosive magnitude for historical volcanism. *J Geophys Res* **87**, 1231-1238 (1982).
2. M. P. McCormick, L.W. Thomason, C.R. Trepte, Atmospheric Effects of the Mt-Pinatubo Eruption. *Nature* **373**, 399–404 (1995).
3. M. Fujiwara et al., Global temperature response to the major volcanic eruptions in multiple reanalysis data sets. *Atmos Chem Phys* **15**, 13507–13518 (2015).
4. C. Oppenheimer, Ice core and palaeoclimatic evidence for the timing and nature of the great mid-13th century volcanic eruption. *Int J Climatol* **23**, 417–426 (2003).
5. C. Oppenheimer, Eruption politics. *Nature Geosci* **8**, 244–245 (2015).
6. P. Sheets, "Introduction" in Archaeology and Volcanism in Central America, P. D. Sheets, Eds (University of Texas Press, 1983), pp. 1-13.
7. S. Shibata, S. Kitamura, A. Ichikawa, A. "Reconsideración del fechamiento de TBJ desde el punto de vista estratigráfico" in En XXIII Simposio de Investigaciones Arqueológicas en Guatemala, B. Arroyo, A. Linares, L. Paiz, Eds (Museo Nacional de Arqueología y Etnología, Guatemala, 2010), pp. 826-838.
8. D. J. Kennett et al., Development and disintegration of Maya political systems in response to climate change. *Science* **338**, 788-791 (2012).
9. J. Lexa, J. Sebesta, J.A. Chavez, W. Hernandez, Z. Pecskey, Geology and volcanic evolution in the southern part of the San Salvador Metropolitan Area. *J Geosci* **56**, 106-140 (2011).
10. I. Suñe-Puchol et al., The Ilopango caldera complex, El Salvador: Origin and early ignimbrite-forming eruptions of a graben/pull-apart caldera structure. *J Volcanol Geoth Res* **371**, 1–19 (2019).
11. C. U. Hammer, H. B. Clausen, W. Dansgaard, Greenland Ice-Sheet Evidence of Post-Glacial Volcanism and Its Climatic Impact. *Nature* **288**, 230–235 (1980).
12. F. Lavigne et al., Source of the great AD 1257 mystery eruption unveiled, Samalas volcano, Rinjani Volcanic Complex, Indonesia. *Proc Natl Acad Sci USA* **110**, 16742-16747 (2013).
13. M. Sigl et al., Timing and climate forcing of volcanic eruptions for the past 2,500 years. *Nature* **523**, 543-549 (2015).
14. R. A. Dull et al., Radiocarbon and geologic evidence reveal Ilopango volcano as source of the colossal 'mystery' eruption of 539/40 CE. *Quat Sci Rev* **222**, 105855 (2019).
15. H. Earnest, *A Reappraisal of the Ilopango Volcanic Eruption in Central El Salvador* (Harvard University, 1999).

16. S. J. Johnsen *et al.*, Oxygen isotope and palaeotemperature records from six Greenland ice-core stations: Camp Century, Dye-3, GRIP, GISP2, Renland and NorthGRIP. *J Quat Sci* **16**, 299–307 (2001).
17. H. Williams, H. Meyer-Abich, *Volcanism in the Southern Part of El Salvador: With Particular Reference to the Collapse Basins of Lakes Coatepeque and Ilopango* (University of California Press, 1955).
18. W. J. Hart, V. Steen-McIntyre, “Tierra Blanca Joven Tephra from the AD 260 eruption of Ilopango caldera” in *Archeology and Volcanism in Central America* (University of Texas Press, 1983), pp. 15–34.
19. D. Pedrazzi, *et al.*, The Ilopango Tierra Blanca Joven (TBJ) eruption, El Salvador: Volcano-stratigraphy and physical characterization of the major Holocene event of Central America. *J Volcanol Geoth Res* **377**, 1–22 (2019).
20. H. Neff, P. Sheets, P. “Archaeological applications of tephra analysis by LA-ICP-MS” in *Laser Ablation-ICP-MS in Archaeological Research*, R.J. Speakman, H. Neff, Eds (University of New Mexico Press, 2005), pp. 117–124.
21. A. Folch, A. Costa, G. Macedonio, FALL3D: a computational model for transport and deposition of volcanic ash. *Comput Geosci* **35**, 1334–1342 (2009).
22. A. Costa *et al.*, Quantifying volcanic ash dispersal and impact of the Campanian Ignimbrite super-eruption. *Geophys Res Lett* **39**, L10310 (2012).
23. A. Costa, V.C. Smith, G. Macedonio, N.E. Matthews, The magnitude and impact of the Youngest Toba Tuff super-eruption. *Front Earth Sci* **2**, 16 (2014).
24. A. Costa, A. Folch, G. Macedonio, Density-driven transport in the umbrella region of volcanic clouds: implications for tephra dispersion models. *Geophys Res Lett* **40**, 4823–4827 (2013).
25. M. Poret, A. Costa, A. Folch, A. Martí, A., Modelling tephra dispersal and ash aggregation: The 26<sup>th</sup> April 1979 eruption, La Soufrière St. Vincent. *J Volcanol Geoth Res* **347**, 207–220 (2017).
26. P.J. Reimer *et al.*, IntCal13 and Marine13 Radiocarbon Age Calibration Curves 0–50,000 Years cal BP. *Radiocarbon* **55**, 1869–1887 (2013).
27. C. Bronk Ramsey, Dealing with outliers and offsets in radiocarbon dating. *Radiocarbon* **51**, 1023–1045 (2009).
28. C. Bronk Ramsey, Methods for Summarizing Radiocarbon Datasets. *Radiocarbon* **59**, 1809–1833 (2017).
29. A.G. Hogg *et al.*, SHCal13 Southern Hemisphere Calibration, 0–50,000 Years Cal BP. *Radiocarbon* **55**, 1889–1903 (2013).
30. Q. Hua, M. Barbetti, A.Z. Rakowski, Atmospheric Radiocarbon for the Period 1950–2010. *Radiocarbon* **55**, 2059–2072 (2013).
31. E.J. Marsh *et al.*, IntCal, SHCal, or a Mixed Curve? Choosing a <sup>14</sup>C Calibration Curve for Archaeological and Paleoenvironmental Records from Tropical South America. *Radiocarbon* **60**, 925–940 (2018).
32. L. Marshall *et al.*, Multi-model comparison of the volcanic sulfate deposition from the 1815 eruption of Mt. Tambora. *Atmos Chem Phys* **18**, 2307–2328 (2018).
33. M. Toohey, M. Sigl, Ice core-inferred volcanic stratospheric sulfur injection from 500 BCE to 1900 CE. *Earth Syst Sci Data* **9**, 809–831 (2017).
34. B.G. Koffman, K.J. Kreutz, A.V. Kurbatov, N.W. Dunbar, Impact of known local and tropical volcanic eruptions of the past millennium on the WAIS Divide microparticle record. *Geophys Res Lett* **40**, 4712–4716 (2013).

35. J. Cole-Dai *et al.*, Cold decade (AD 1810-1819) caused by Tambora (1815) and another (1809) stratospheric volcanic eruption. *Geophys Res Lett* **36** (2009).
36. A. J. Bourne *et al.*, Underestimated risks of recurrent long-range ash dispersal from northern Pacific Arc volcanoes. *Sci Rep* **6**, 29837 (2016).
37. C. Sun *et al.*, Ash from Changbaishan Millennium eruption recorded in Greenland ice: Implications for determining the eruption's timing and impact. *Geophys Res Lett* **41**, 694–701 (2014).
38. C. T. Plummer *et al.*, An independently dated 2000-yr volcanic record from Law Dome, East Antarctica, including a new perspective on the dating of the 1450s CE eruption of Kuwae, Vanuatu. *Clim Past* **8**, 1929-1940 (2012).
39. E. Gautier *et al.*, 2600-years of stratospheric volcanism through sulfate isotopes. *Nat Commun* **10** (2019).
40. M. Sigl *et al.*, Insights from Antarctica on volcanic forcing during the Common Era. *Nat Clim Change* **4**, 693-697 (2014).
41. L. J. Lucke, G. C. Hegerl, A. Schurer, R. Wilson, Effects of Memory Biases on Variability of Temperature Reconstructions. *J Climate* **32**, 8713-8731 (2019).
42. F. Zhu, J. Emile-Geay, G. J. Hakim, J. King, K. J. Anchukaitis, Resolving the Differences in the Simulated and Reconstructed Temperature Response to Volcanism. *Geophys Res Lett* **47**, e2019GL086908 (2020)
43. M. Toohey, K. Kruger, C. Timmreck, Volcanic sulfate deposition to Greenland and Antarctica: A modeling sensitivity study. *J Geophys Res-Atmos* **118**, 4788-4800 (2013).
44. L. Marshall *et al.*, Exploring How Eruption Source Parameters Affect Volcanic Radiative Forcing Using Statistical Emulation. *J Geophys Res-Atmos* **124**, 964-985 (2019).
45. R. Neukom *et al.*, Inter-hemispheric temperature variability over the past millennium. *Nat Clim Change* **4**, 362-367 (2014).
46. S.E. Metcalfe, J.A. Barron, S.J. Davies, The Holocene history of the North American Monsoon: 'known knowns' and 'known unknowns' in understanding its spatial and temporal complexity. *Quat Sci Rev* **120**, 1-27 (2015).
47. J.W. Webster *et al.*, Stalagmite evidence from Belize indicating significant droughts at the time of Preclassic Abandonment, the Maya Hiatus, and the Classic Maya collapse. *Palaeogeogr Palaeocl* **250**, 1-17 (2007).
48. S. Duggen *et al.*, The role of airborne volcanic ash for the surface ocean biogeochemical iron-cycle: a review. *Biogeosciences* **7**, 827–844 (2010).
49. J.F. Luhr, W.G. Melson, "Mineral and glass compositions in June 15, 1991, pumices: Evidence for dynamic disequilibrium in the dacite of Mount Pinatubo" in *Fire and Mud: Eruptions and Lahars of Mount Pinatubo, Philippines*, C.G. Newhall, Punongbayan, R.S., Eds (University of Washington Press, 1996), pp. 733-750.
50. J.L. Sarmiento, Atmospheric CO<sub>2</sub> stalled. *Nature* **365**, 697-698 (1993).
51. O. Arnalds "The influence of Volcanic Tephra (Ash) on ecosystems" in *Advance in Agronomy*, D. Sparks, Ed (Elsevier, 2013), pp. 331–380.
52. M. Poret *et al.*, Modeling eruption source parameters by integrating field, ground-based and satellite-based measurements: The case of the 23 February 2013 Etna paroxysm. *J Geophys Res- Sol Ea* **123**, 5427-5450 (2018).
53. I. Aida, Reliability of a tsunami source model derived from fault parameters. *J Phys Earth* **26**, 57–73 (1978).
54. W. Cornell, S. Carey, H. Sigurdsson, Computer simulation of transport and deposition of Campanian Y-5 ash, *J Volcanol Geoth Res* **17**, 89–109 (1983).

55. A. Folch, A. Costa, A. Durant, G. Macedonio, A model for wet aggregation of ash particles in volcanic plumes and clouds: 2. Model application, *J Geophys Res* **115**, B09202 (2010).
56. L. J. Connor, C.B. Connor, "Inversion is the key to dispersion: understanding eruption dynamics by inverting tephra fallout" in Statistics in Volcanology H. M. Mader, S. G. Coles, C. B. Connor, L. J. Connor, Eds (The Geological Society, 2006), pp. 231-242.
57. J.R. McConnell et al., Lead pollution recorded in Greenland ice indicates European emissions tracked plagues, wars, and imperial expansion during antiquity. *Proc Natl Acad Sci USA* **115**, 5726-5731.
58. J. R. McConnell, G.W. Lamorey, S.W. Lambert, K.C. Taylor, Continuous Ice-Core Chemical Analyses Using Inductively Coupled Plasma Mass Spectrometry. *Environ Sci Technol* **36**, 7-11 (2002).
59. S.E. Coulter, J.R. Pilcher, V.A. Hall, G. Plunkett, S.M. Davies, Testing the reliability of the JEOL FEGSEM 6500F electron microprobe for quantitative major element analysis of glass shards from rhyolitic tephra. *Boreas* **39**, 163-169 (2010).

**Figure 1.** The location of the Ilopango caldera in El Salvador (red triangle) with the TBJ tephra thicknesses (data from ref. 19 and 20). (A) Tephra thickness (mm) within ~80 km of the vent. Centimeters of ash were deposited in parts of Mexico (A) while areas closer to the vent (B) were covered with decimeters of ash and PDCs. The tree stump that was radiocarbon dated (Fig. 2) was found within the PDC deposits at the location marked with a black star; the location of Chalchuapa (El Salvador) is marked by a white star. (C) The TBJ tephra is ~20 cm thick in the Casa Blanca archeological sites in Chalchuapa. (D) The ~2 m thick TBJ deposits ~10 km west of the vent (grey star in B). Most of the deposit is PDC but there are a few centimeters of fallout at the base, which blankets soil that had been worked by the Maya. (E) The glass shards from the TBJ eruption that were identified in the TUNU2013 ice core from Greenland.

**Figure 2.** (A) A photograph of the cross section through the Mahogany tree that was felled by the TBJ PDCs and recovered from within the deposits ~25 km from the volcano (Fig. 1B). Radiocarbon measurements were carried out on samples from two sections (labelled A and B in white) that extend from the pith to the bark edge, and each contiguous sample spans approximately 5 or 10 years (*Gap*). (B) The radiocarbon data from the samples taken through Section A (bottom) and Section B (top) were modeled onto the IntCal13 radiocarbon calibration curve (26) using a Bayesian statistical approach, which takes into account the order of the dates (older pith at the bottom to bark edge at the top), in OxCal v.4.3.2 (28) to determine calendar dates (Table 1). The distributions (likelihoods) for the single calibrated dates are shown in light grey, while the marginal posterior distributions (95.4% probability) that take into account other dates in the sequence are shown in darker grey. (C) The two determinations of the modeled date at the bark edge (i.e. felling dates in B) were combined in OxCal to provide an eruption date of 425-440 CE (95.4% probability).

**Figure 3.** (A) Ice core non sea-salt sulfur (nssS) data from Greenland (North Greenland Eemian Ice Drilling (NEEM) cores) and Antarctica (West Antarctic Ice Sheet Divide Core (WDS) and the B40 core from Dronning Maud Land), modified from ref. (13). The large volcanic nssS signals (13) are labelled with the calendar year that marks the start of volcanic sulfate deposition. The nssS peaks at 432 CE in Greenland and 434 CE in Antarctica (marked with a double headed arrow) are within the new radiocarbon date range for the TBJ eruption (Fig. 2; Table 1). (B) Particle concentrations and nssS data from the TUNU2013 ice core from Greenland (Fig. 1) spanning

429.5 to 434 CE. The peak in particles (solid line = 4.5-9.5  $\mu\text{m}$ ; dashed= 2.4-4.5  $\mu\text{m}$  fraction) is centered at 431 CE, while the nssS starts to be deposited a year later as it takes longer for it to be deposited from the stratosphere (32). The TUNU2013 glass shards (Fig. 1) that were analyzed (Fig. 5) were extracted from the 431 CE ice sample.

**Figure 4.** Glass major elements geochemical data from the TBJ deposits (red triangles; data from ref. 19), and glass shards from the TUNU2013 ice core located at a depth that corresponds to 431 CE (black squares). Error bars on (A) represent  $\pm 1$  standard deviation of repeat analyses of a reference glass (see *SI Appendix*; SID1 dataset), and errors are smaller than the data points on (B).

**Table 1: Radiocarbon determinations of samples taken across sections (A and B) from pith (4) to the bark edge (1) of the tree found within the TBJ PDC (see Figure 2).**

Trunk 1, Section	Sample name	Lab code (GrM-)	%C	$\delta^{13}\text{C}$ (‰)	$\pm$	Acorr (%)	$\pm$ (1 $\sigma$ )	$^{14}\text{C}$ Age (yr BP)	$\pm$ (1 $\sigma$ )	Modelled radiocarbon date (CE) at 95.4% probability	
A	A1	15054	39.1	-24.53	0.21	82.06	0.20	1588	20	425	446
	A1 DUPLICATE	15055	38.1	-24.60	0.21	82.01	0.19	1593	19		
	A2	15056	40.4	-26.15	0.21	81.67	0.19	1627	19	420	441
	A3	15058	39.5	-27.02	0.21	81.83	0.20	1611	19	400	421
	A3 DUPLICATE	15060	40.9	-27.20	0.21	81.80	0.21	1614	20		
	A4	15061	39.8	-27.26	0.21	81.51	0.20	1642	20	390	411
B	B1	15063	38.7	-25.32	0.21	81.75	0.20	1618	20	413	435
	B2	15196	38.8	-26.27	0.21	81.79	0.20	1615	19	403	425
	B2 DUPLICATE	15197	38.7	-26.85	0.26	81.69	0.20	1624	19		
	B3	15198	38.5	-27.24	0.26	81.46	0.20	1647	19	393	415
	B4	15200	37.5	-26.89	0.26	81.51	0.20	1642	19	383	405

Note: Duplicate analyses were combined in the OxCal model.

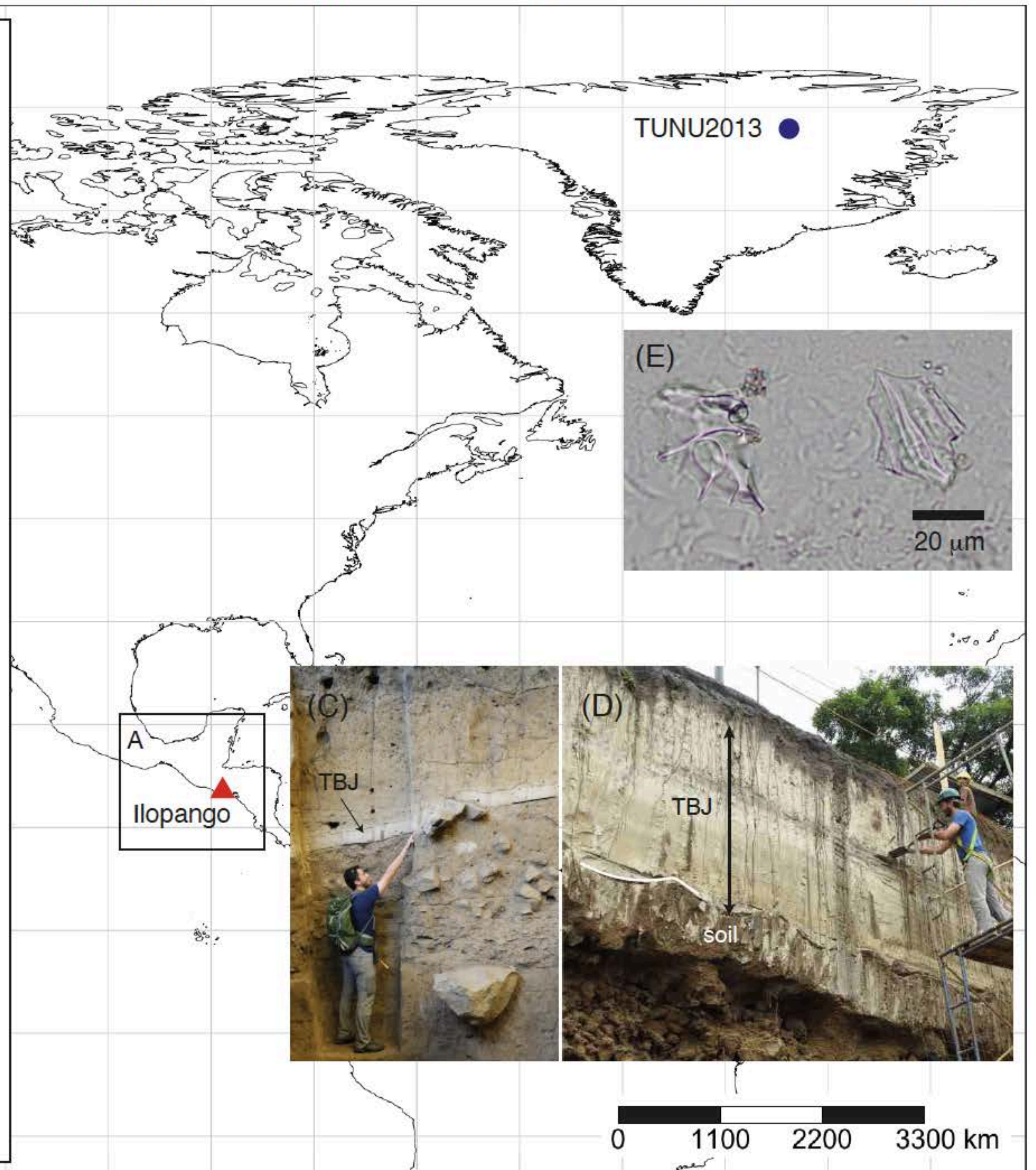
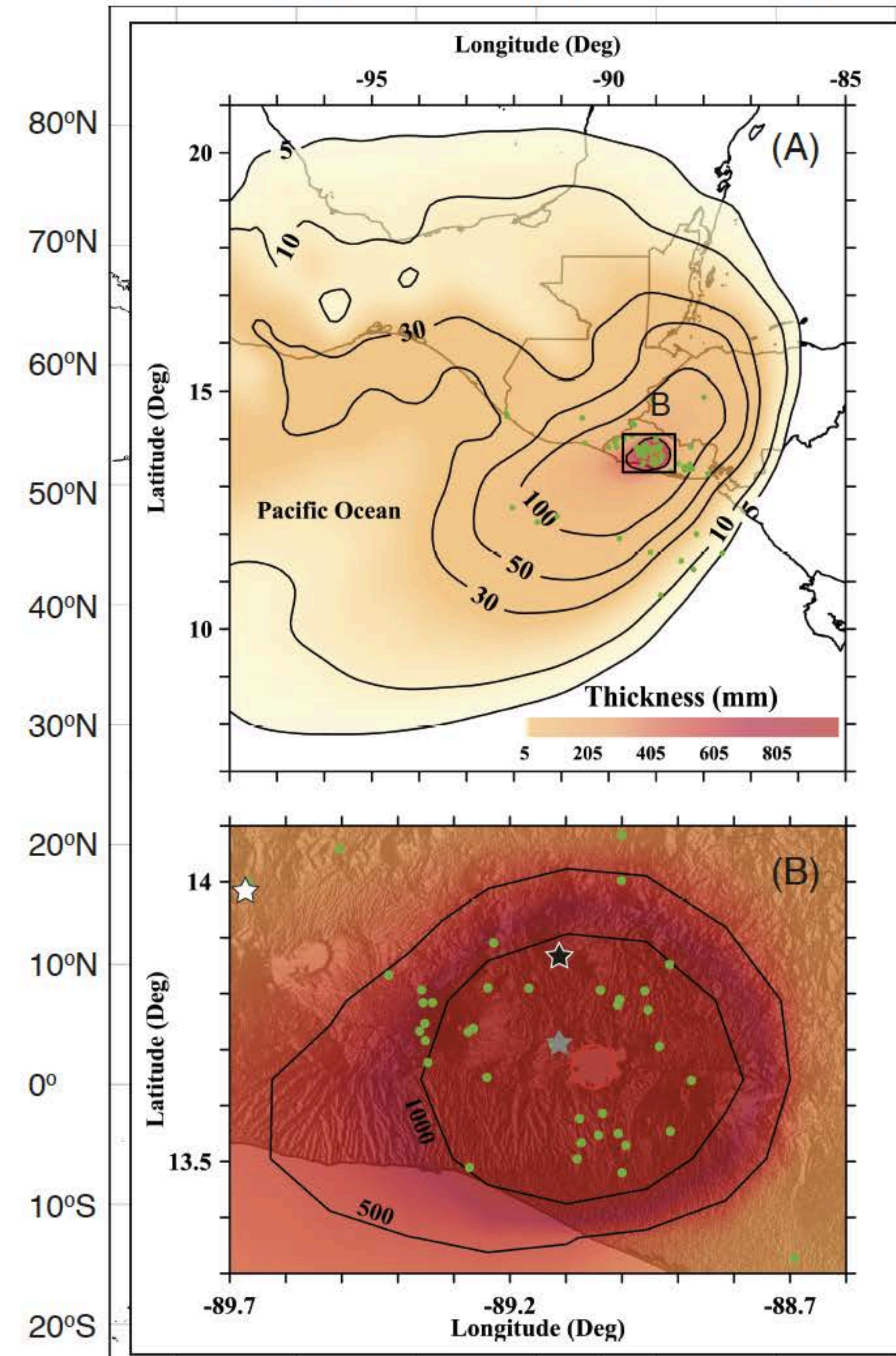
Table 2: Major element compositions (normalized to 100%) of glass shards in the TUNU2013 ice core (Greenland) at 431 CE compared to those in the TBJ eruption deposits

	SiO <sub>2</sub>	TiO <sub>2</sub>	Al <sub>2</sub> O <sub>3</sub>	FeOt	MnO	MgO	CaO	Na <sub>2</sub> O	K <sub>2</sub> O	Cl	Analytical total	<i>n</i> <sup>^</sup>
<b>TUNU2013, 431 CE</b>												
QUB-1983-2	76.39	0.27	13.17	1.06	0.06	0.30	1.18	4.42	3.00	0.15	96.96	
QUB-1983-10	76.22	0.29	13.30	0.95	0.06	0.31	1.23	4.42	3.00	0.21	95.43	
QUB-1983-3	76.80	0.18	13.19	1.19	0.12	0.28	1.18	3.66	3.05	0.34	91.25	
QUB-1983-4	76.08	0.21	13.37	1.06	-0.05	0.23	1.15	4.80	2.91	0.23	97.45	
QUB-1983-4b	77.19	0.35	13.02	1.03	0.00	0.27	1.25	3.49	3.19	0.21	93.93	
QUB-1983-7	75.76	0.28	13.11	0.97	-0.01	0.27	1.09	5.28	3.07	0.17	97.47	
QUB-1983-6	75.71	0.27	12.88	1.06	0.05	0.24	1.09	5.37	3.13	0.19	96.54	
QUB-1983-21	65.48	0.73	16.14	3.81	0.23	2.27	3.50	5.78	1.87	0.20	96.48	
<b>TBJ</b>												
Rhyolite*	77.14	0.19	12.75	1.19	0.07	0.20	1.23	4.36	2.87	0.20		
	0.46	0.03	0.34	0.10	0.04	0.03	0.09	0.20	0.12	0.02		248
Representative analyses of the less evolved TBJ glasses												
ILO-32_dark-38	58.96	0.65	12.61	7.15	0.26	6.62	9.54	3.07	0.97	0.09	96.10	
ILO-32_grey-2	65.55	0.49	15.60	4.58	0.20	2.63	5.09	3.82	1.68	0.17	92.68	
ILO-32_grey-13	68.56	0.53	15.90	3.28	0.16	0.83	3.54	4.64	2.18	0.14	92.68	

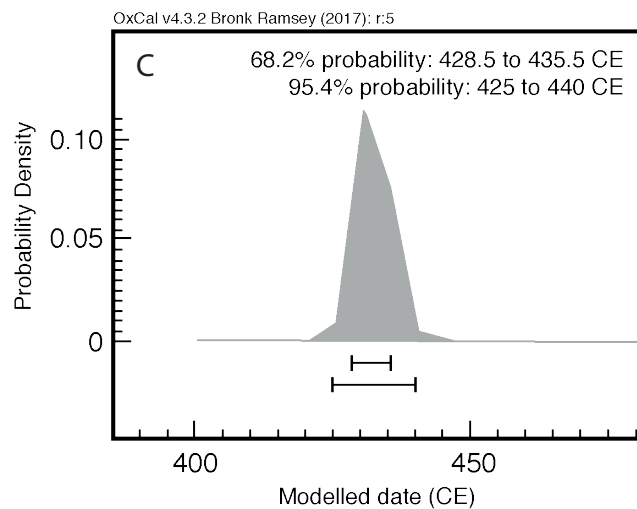
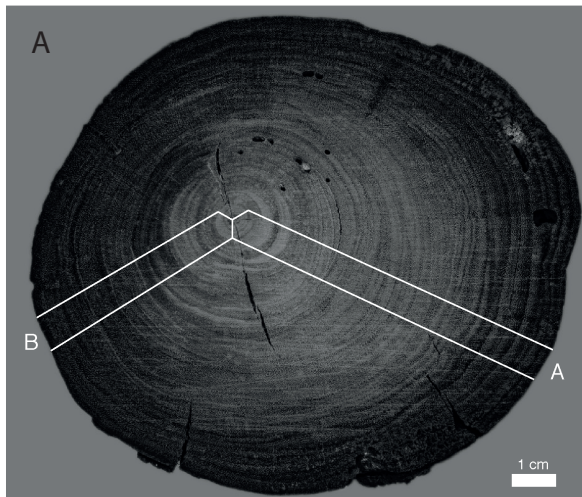
\*average composition of the rhyolite population (Pedrazzi et al., 2019) with <sup>^</sup>*n* for Cl = 150. Analytical total is the original unnormalized value. Reference glass analyses are included in the Supporting Information.



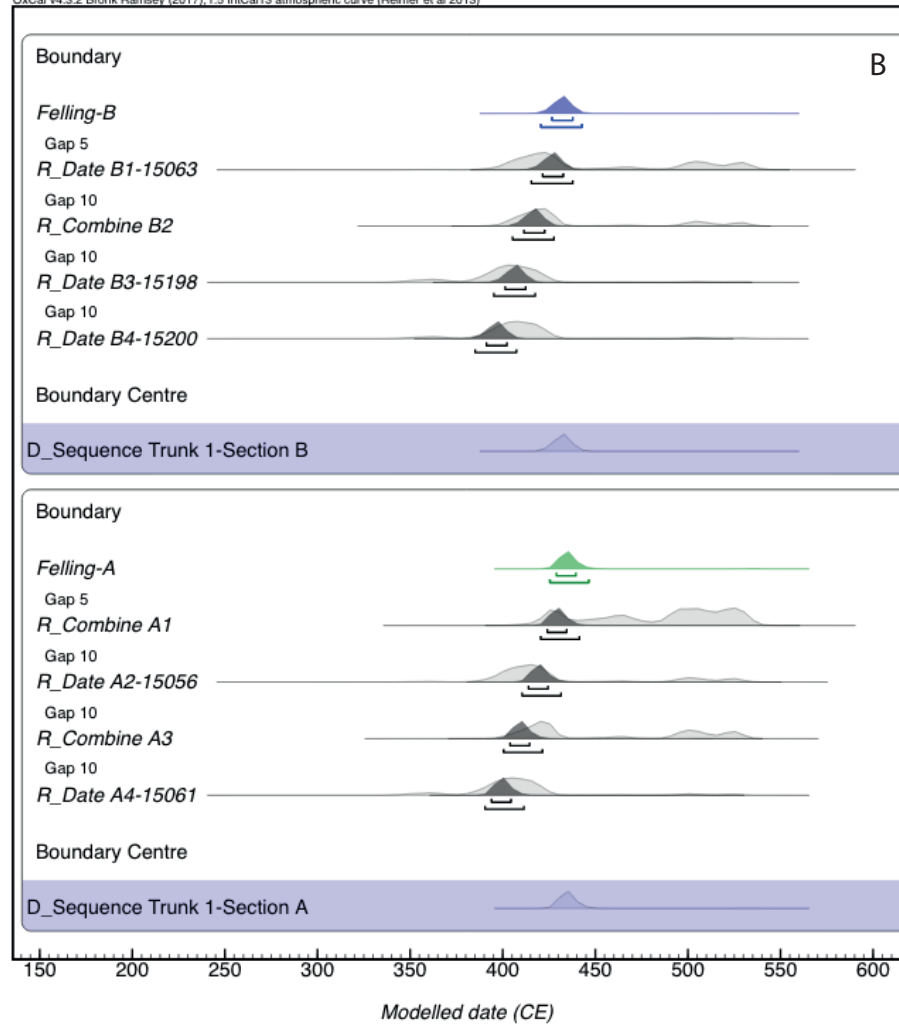
160°W 140°W 120°W 100°W 80°W 60°W 40°W 20°W

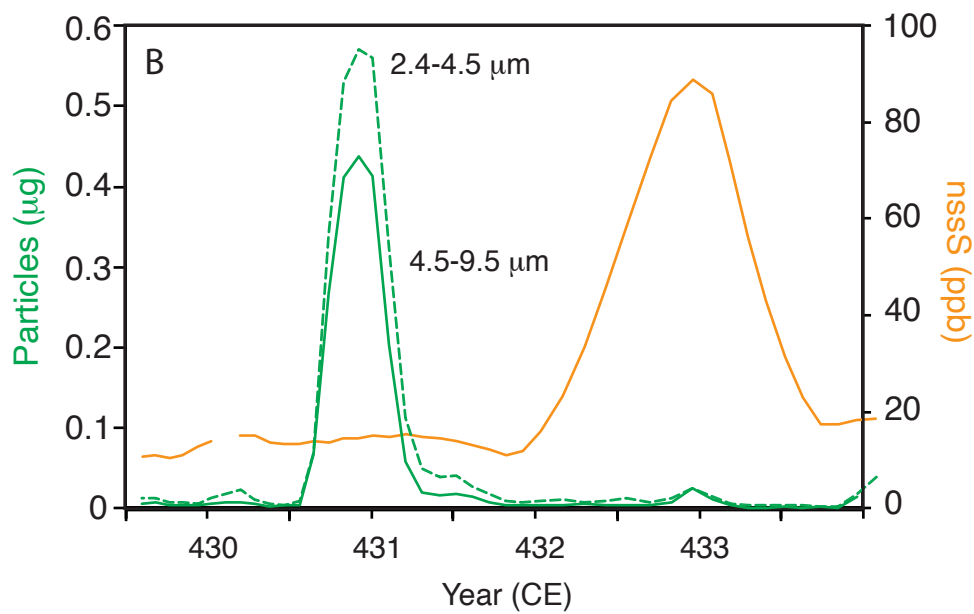
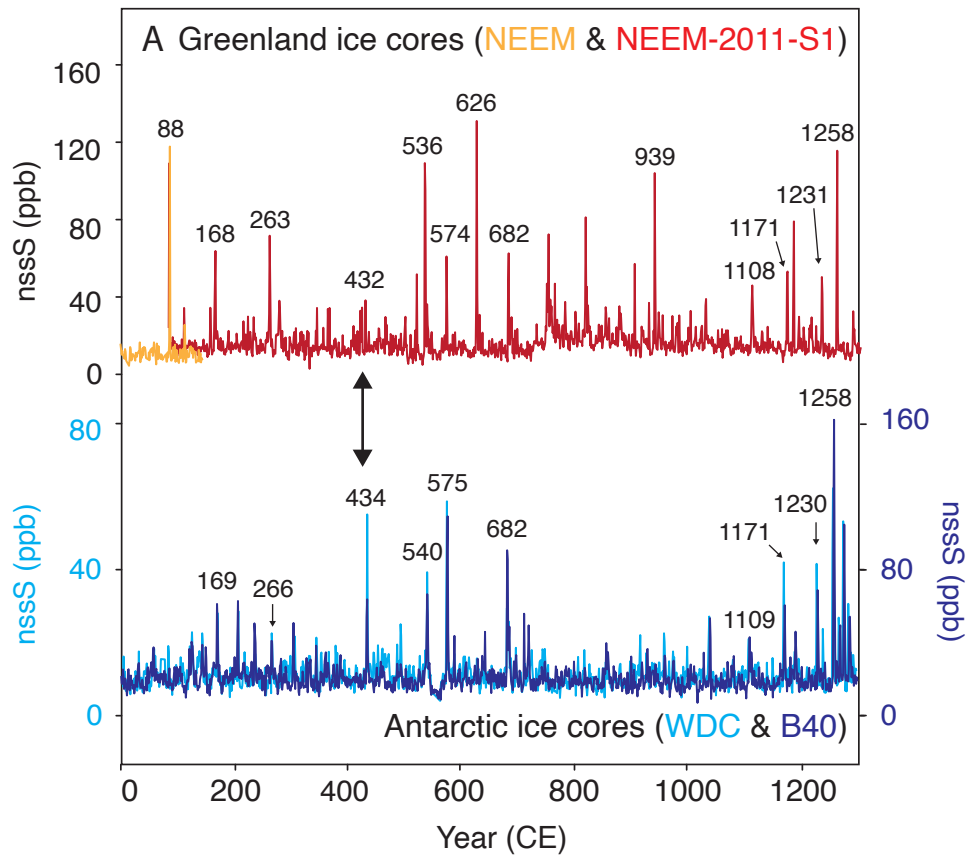


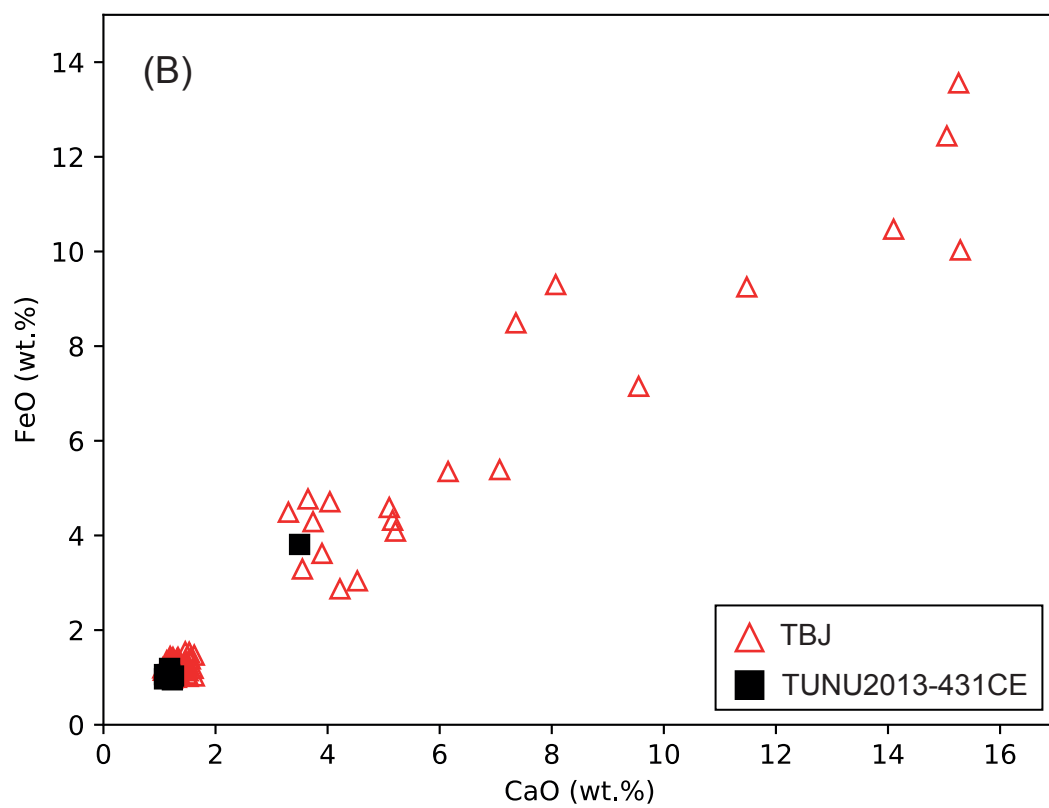
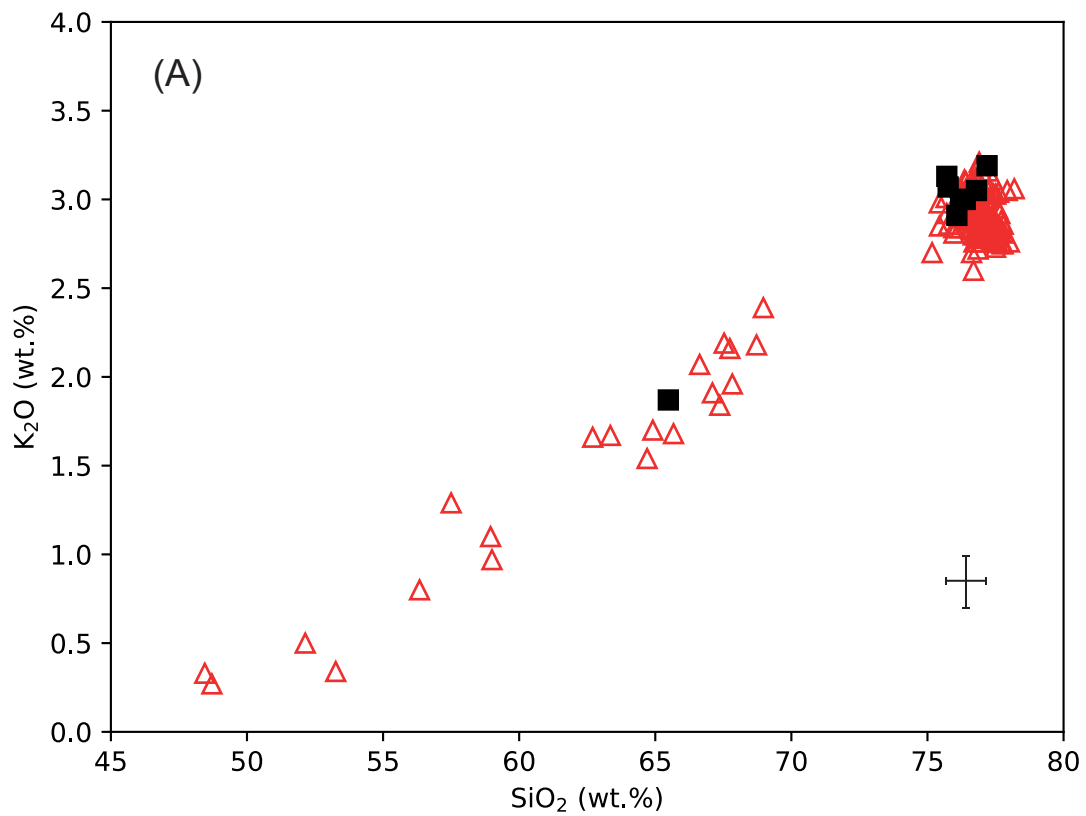




OxCal v4.3.2 Bronk Ramsey (2017): r:5 IntCal13 atmospheric curve (Reimer et al 2013)







## SUPPORTING INFORMATION APPENDIX

### The magnitude and impact of the 431 CE Tierra Blanca Joven eruption of Ilopango, El Salvador

Smith, V.C., Costa, A., Aguirre-Díaz, G., Pedrazzi, D., Scifo, A., Plunkett, G., Poret, M., Tournigand, P.Y., Miles, D., Dee, M., McConnell, J.R., Sunyé-Puchol, I., Dávila Harris, P., Sigl, M., Pilcher, J.R., Chellman, N., Gutiérrez, E.

Corresponding authors: Victoria Smith, [victoria.smith@arch.ox.ac.uk](mailto:victoria.smith@arch.ox.ac.uk) &  
Antonio Costa, [antonio.costa@ingv.it](mailto:antonio.costa@ingv.it)

#### Contents

- Ash dispersal modeling
  - Table S1
  - Figure S1
  - Figure S2
- Radiocarbon chronologies
  - Table S2
  - Figure S3
  - Figure S4
  - Figure S5
- Tephra correlation using glass compositions
  - Figure S6
- Volatile content of the TBJ magma
  - Figure S7

#### Other supporting materials

- Movie - SIM1: Simulated tephra dispersal associated with the 431 CE Tierra Blanca Joven eruption from El Salvador over the 117 hours following the onset of the eruption. The isopachs are in millimeters, which correspond to tephra load in kg/m<sup>2</sup>.
- Dataset - SID1: An excel file with: (1) reference glass analyses for the data presented in Table 2, and (2) volatile data presented in Fig. S7.

---

#### Ash dispersal modeling

The results of the best fit TBJ tephra dispersal inversion are reported in Table S1 and Fig. S1. The first Aida (1) index ( $K$ ), reported in Fig. S1, reflects the geometric average and is 0.99; and the second ( $k$ ), related to the geometric standard deviation is 2.90. The best fit scenario (TBJ-175) corresponds to the meteorological synoptic fields from 21 to 26 February 1997 rotated 5° anti-clockwise around the vent. Although the winds generally blow towards the E, the observed tephra deposits indicate that during the eruption the winds were directed S-SW (see *SI Appendix* SIM1 movie). The mass distribution within the eruptive column was obtained by empirically best-fitting the Suzuki (2) distribution shown in Fig. S2. It mimics the distribution reconstructed by computationally intensive 3D simulations (3). These simulated results are in agreement with the measured thicknesses (Fig. S1). The mean error associated with the erupted mass estimation is about a factor 1.5 and the maximum error is a factor 3.

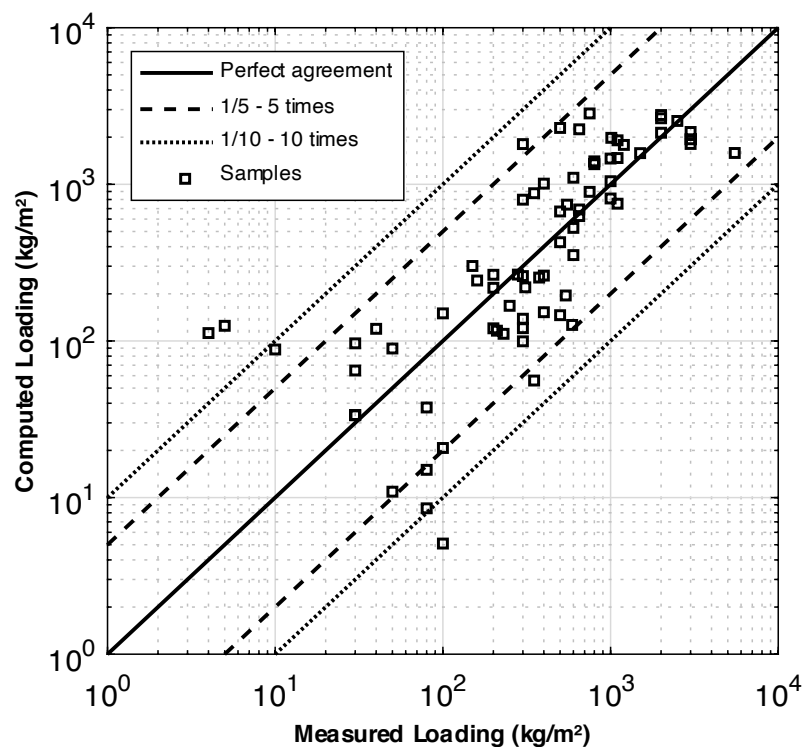
**Table S1.** Best-fit results of tephra dispersal inversion for the TBJ co-ignimbrite phase

Modeled Dispersion Parameters	Explored Range	TBJ-175 <sup>a</sup>
Tephra mass ( $10^{14}$ kg)	Calculated	1.26
Tephra volume DRE ( $\text{km}^3$ )	Calculated	55
Eruption duration (hours)	1-5	1
Mass eruption rate ( $10^{10}$ kg/s)	1-5	3.5
Column height (km)	45-55	45
Suzuki coefficients $A$ (-) <sup>a</sup>	2-9	2
Average deposit density ( $\text{kg/m}^3$ ) <sup>b</sup>	Assumed	1000
Aida indexes $K/k$ (-)	Calculated	0.99/2.90

Footnote: <sup>a</sup> The eruption source is described in a purely empirical way in order to reproduce the optimal geometrical shape of the deposits using the Suzuki distribution (2,4). The eruption column acts as a vertical line source (this simplification is only valid in distal areas).

<sup>b</sup> This value is used to convert deposit thickness, in mass loading, and to calculate total tephra volume from the total mass. A density of  $2300 \text{ kg/m}^3$  was used to convert the tephra volume into a dense rock equivalent (DRE) magma volume.

The *SI Appendix* Movie (SIM1) shows the reconstructed time evolution of the tephra deposition. At proximal locations, 1 cm of tephra was deposited in approximately 4 hours ( $\sim 10$  km from the vent; grey star on Fig. 1B, and deposit is shown in Fig. 1D). Whereas in medial locations, such as the Casa Blanca archaeological site (76 km from the caldera; white star on Fig. 1B), it took  $\sim 7$  hours for 1 cm of ash to accumulate. Most of the millimeter-thick ash deposits found at sites hundreds of kilometers from the caldera would have accumulated within a couple of days.

**Figure S1:** Comparison between the loading from the best-fit FALL3D simulations and the field data at each of the 72 locations. The loading in  $\text{kg/m}^2$  is equivalent to tephra thickness in millimeters.

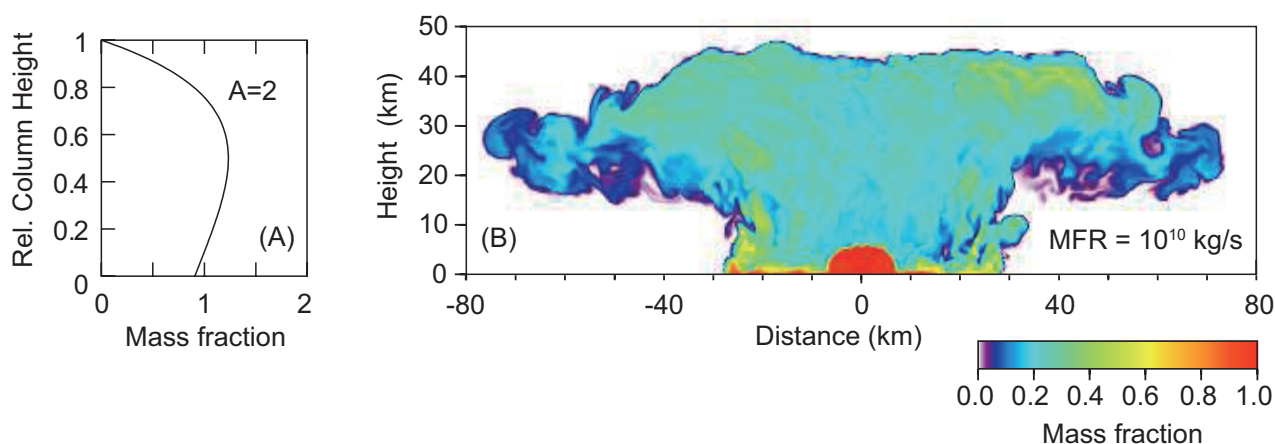


**Figure S2:** (A) The distribution of the total mass within the simulated TBJ column, which corresponds to a Suzuki (2) coefficient,  $A$ , of 2. (B) A cross section through a plume with a Mass Flow Rate of  $1 \times 10^{10}$  kg/s, 800 s after the plume initiation, showing the mass distribution within the plume as simulated by a computational fluid dynamics 3D code. Figure modified after (3).

### Radiocarbon chronologies

We collated published radiocarbon data related to the TBJ (Table S2; data from refs. 5-8) and ran it in an OxCal Bayesian model with outlier analysis. We used a *Sequence* model which considers the stratigraphic positions of samples (i.e., pre-TBJ, within the TBJ deposit, and post-TBJ) to help constrain the date.

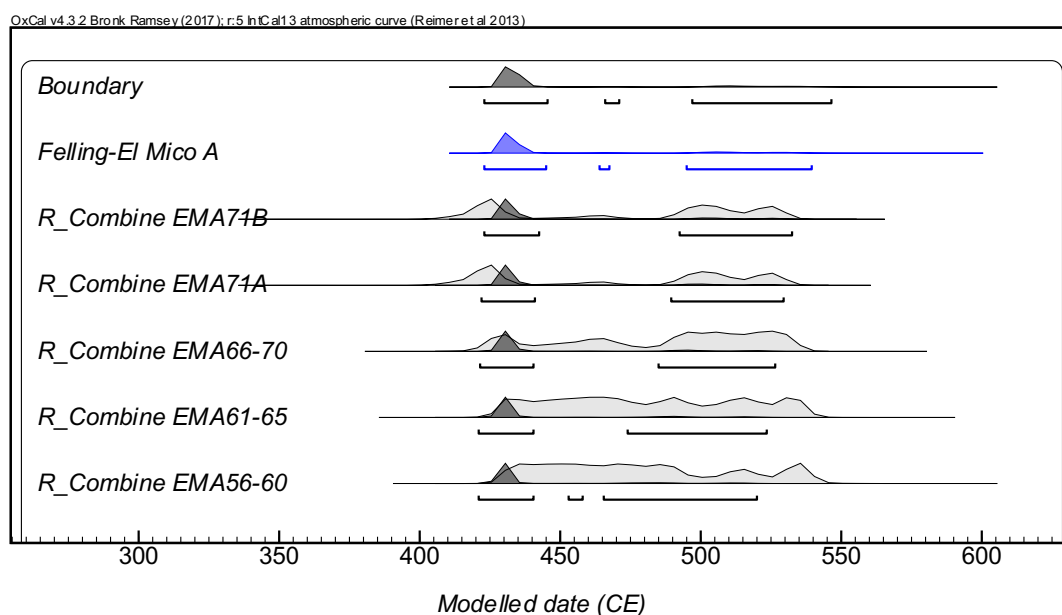
The tree stump was recovered from within a TBJ PDC deposit at Wazapa Hacienda El Mico (location 352-A; N13.89465, W89.16584; ~358 m above sea level) approximately 25 km NNW of Ilopango. The tree is from the mahogany family (i.e. Meliaceae). It is slightly charred and rings can be observed within a cross section (Fig. 2), with 24-37 rings distinguished from the pith through to the bark edge. The ring boundaries are not particularly clear and they are not uniform around the pith so we are unsure whether the rings represent seasonally variation. Furthermore, there is not strong seasonality experienced at similar locations and such elevations today so the numbers of rings are likely to be underrepresented and thus, underestimate the age of the tree. We tested the sensitivity of the radiocarbon model and the following results were obtained: 433-452 CE if rings are 1.5 times those counted, and 447-474 CE if number of rings are doubled.

Studies of the Bomb enrichment of  $^{14}\text{C}$  allows three zones to be defined in both hemispheres, with 1 closest to the poles and 3 extending to the equator. El Salvador is in Zone NH2, and IntCal13 is the correct curve to use for radiocarbon calibration (9). The Dull et al. (10) radiocarbon data were recalibrated using the IntCal13 curve (Fig. S3-S5). The range of dates are slightly older than dates calculated with the mixed calibration curve. If the felling ages of the 4 datasets (10) are combined within a single OxCal model the date of the eruption is either at 401-431 CE or 471-530 CE (95.4% probability range).

**Table S2.** Modeled and recalibrated (using IntCal13; 11) radiocarbon data relating to the TBJ deposits.

Laboratory code	<sup>14</sup> C	±	Ref.	Sample information	Outlier probability (%)^	Modeled radiocarbon date (CE) at 95.4% probability	
Above TBJ							
PLD-28988	1605	20	8		5	403	535
Eruption						400	525
Within TBJ deposits							
CAMS-78595	1810	40	7	Seed	5	270	446
CAMS-78600	1780	50	7	Charcoal	5	272	414
CAMS-46574	1590	50	10	Tree	5	348	500
CAMS-46575	1610	50	10	Tree	5	340	500
Tx3122	1630	70	5*	Charcoal <sup>\$</sup>	10	293	501
Tx3114	1940	50	5*	Charcoal	5	270	486
P-1803	1710	60	5*	Charcoal (reworked?) <sup>\$</sup>	10	270	430
Hv5001	1450	310	5*	Small charcoal	10	283	492
Hv5004	1925	215	5*	Small charcoal	10	272	478
Hv2534	1660	95	5*	Charcoal <sup>\$</sup>	10	279	483
Hv2535	1525	70	5*	Charcoal <sup>\$</sup>	10	344	502
Hv264	1690	85	5*	Charcoal <sup>\$</sup>	10	274	471
Hv5002	1590	70	5*	Charcoal <sup>\$</sup>	10	329	504
Below TBJ							
Tx2324	1970	60	5	Soil <sup>\$</sup>	10	184	397
PLD-28989	1720	20	8		5	246	392
CAMS-60527	1610	50	6	Peat	5	231	398

Footnote: \* quoted in reference (ref.) 6; <sup>^</sup>estimated based on known information, i.e., those where the stratigraphic position is not confirmed were assigned a higher probability of being outliers; <sup>\$</sup> stratigraphic position is inferred. Values in grey italics are outliers in the model.



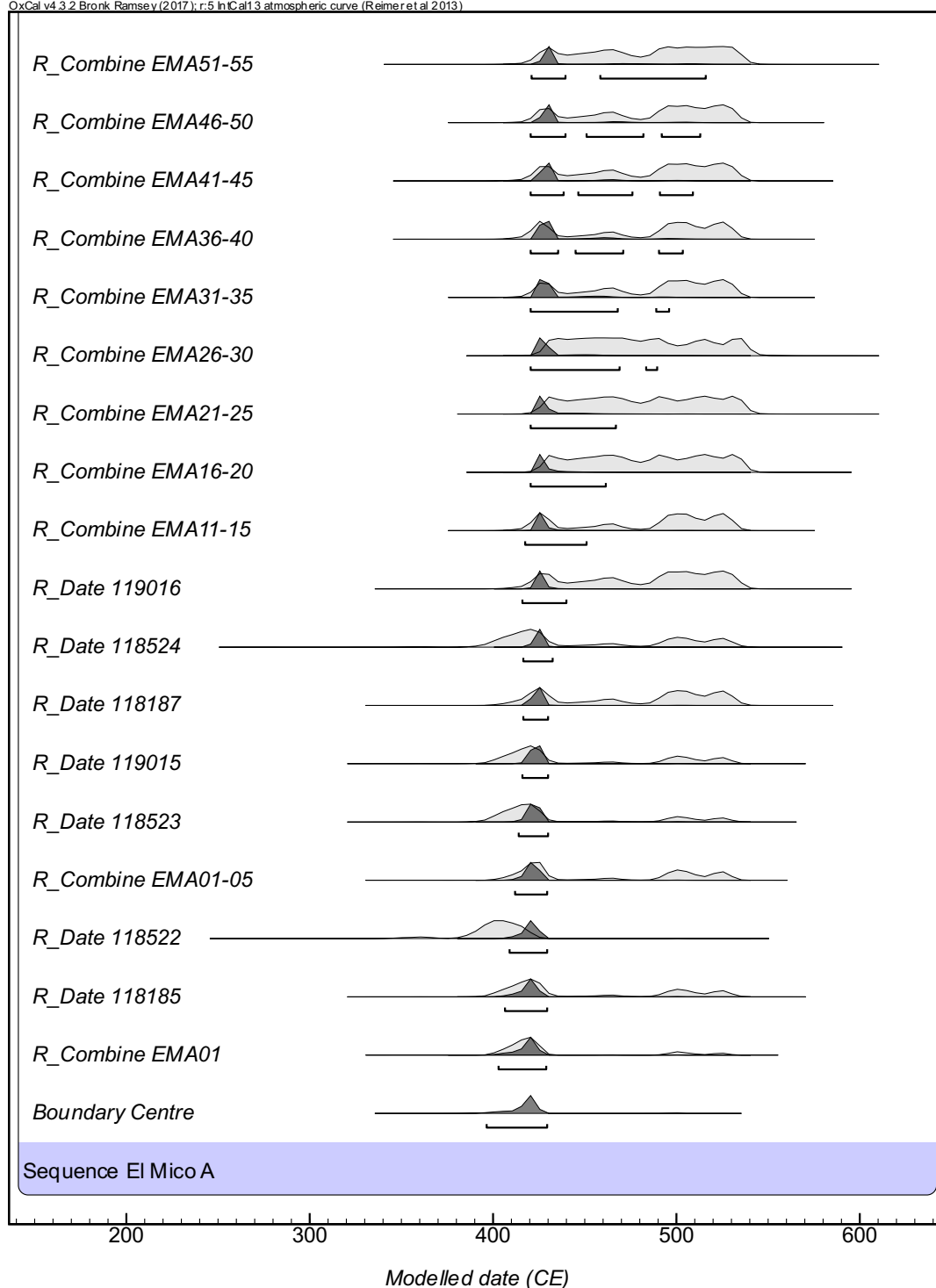


**Figure S3:** Recalibration of the El Mico A radiocarbon data (6) using IntCal13 (11) in OxCal (12). The 95.4% probability range of the felling (eruption) date for El Mico A is: 423-445 CE (78.3%), 464-467 CE (0.5%) and 495-539 CE (16.6%).



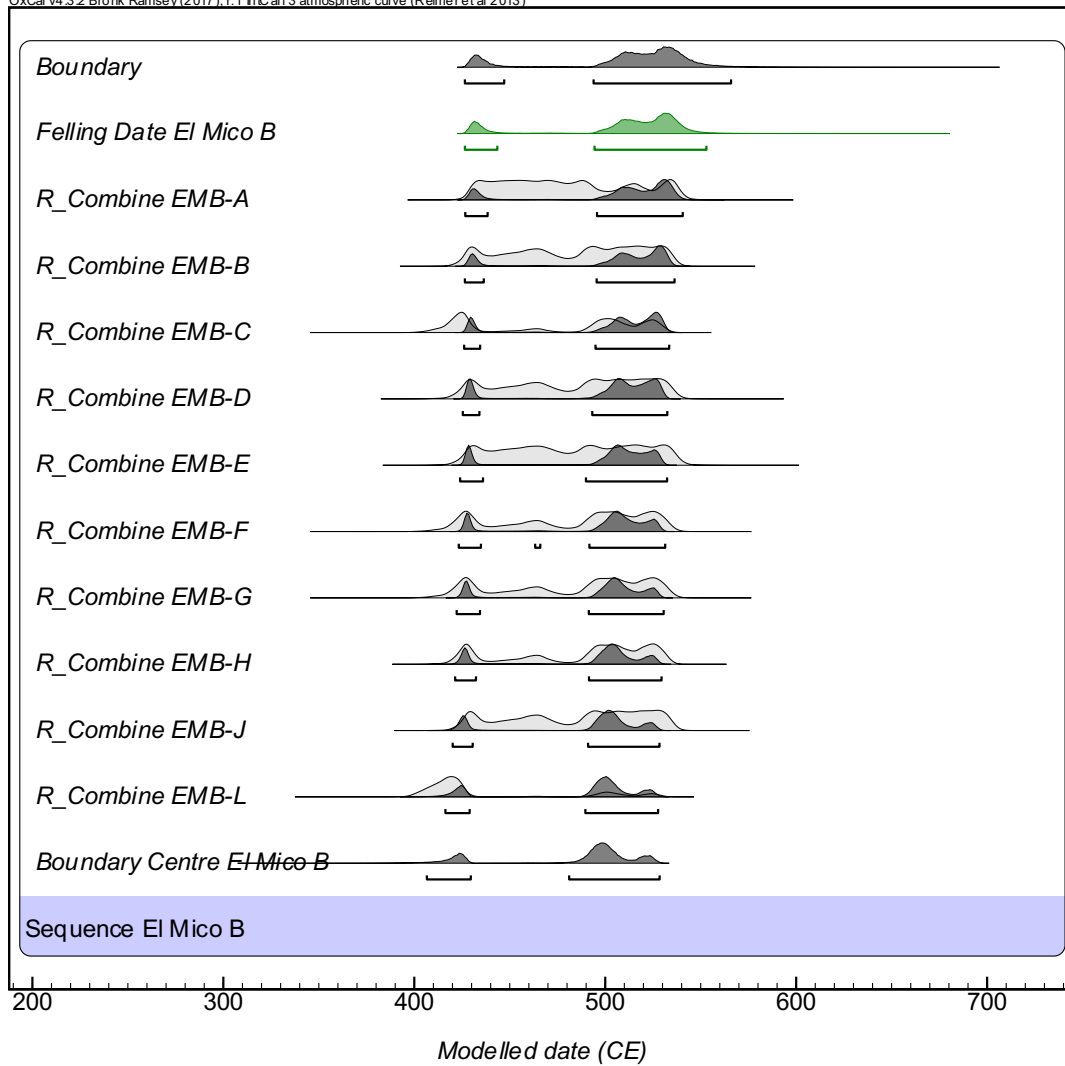


**Figure S4:** Recalibration of the El Mico B radiocarbon data (6) using IntCal13 (11) in OxCal (12). The 95.4% probability range of the felling (eruption) date for El Mico B is: 426-443 CE (13.8%) and 494-553 (81.6%).

We compared the glass compositions of the TUNU2013 431 CE sample to other known Northern Hemisphere eruptions around the same time, which include the: TBJ (425-440 CE at 95.4% probability); 472 CE Pollena eruption from Vesuvius, Italy (13); and the KS1 eruption of Ksudach (245-360 CE; 95.4% probability), KL-UK-1 eruption of Kliuchevskoi (325-611 CE; 95.4% probability), and SH#12 eruption of Shiveluch (542-639 CE; 95.4% probability) in Kamchatka, Russia (14). The Shiveluch SH#12 glasses are identical in composition to most of the TUNU2013 431 CE glasses, apart from very slightly lower CaO contents, and the Shiveluch glasses do not extend to less evolved compositions as seen in the ice core sample and the TBJ glasses (Fig. S6). The SH#12 Shiveluch eruption is unlikely to be the source of the tephra at 431 CE and the nssS peak in the TUNU2013 ice core as it occurred >100 years later (542-639 CE at 95.4% probability) (14), and the contemporaneous nnsS peak in the Antarctic ice cores confirms that the 431 CE eruption occurred in the tropics (discussed in the paper).

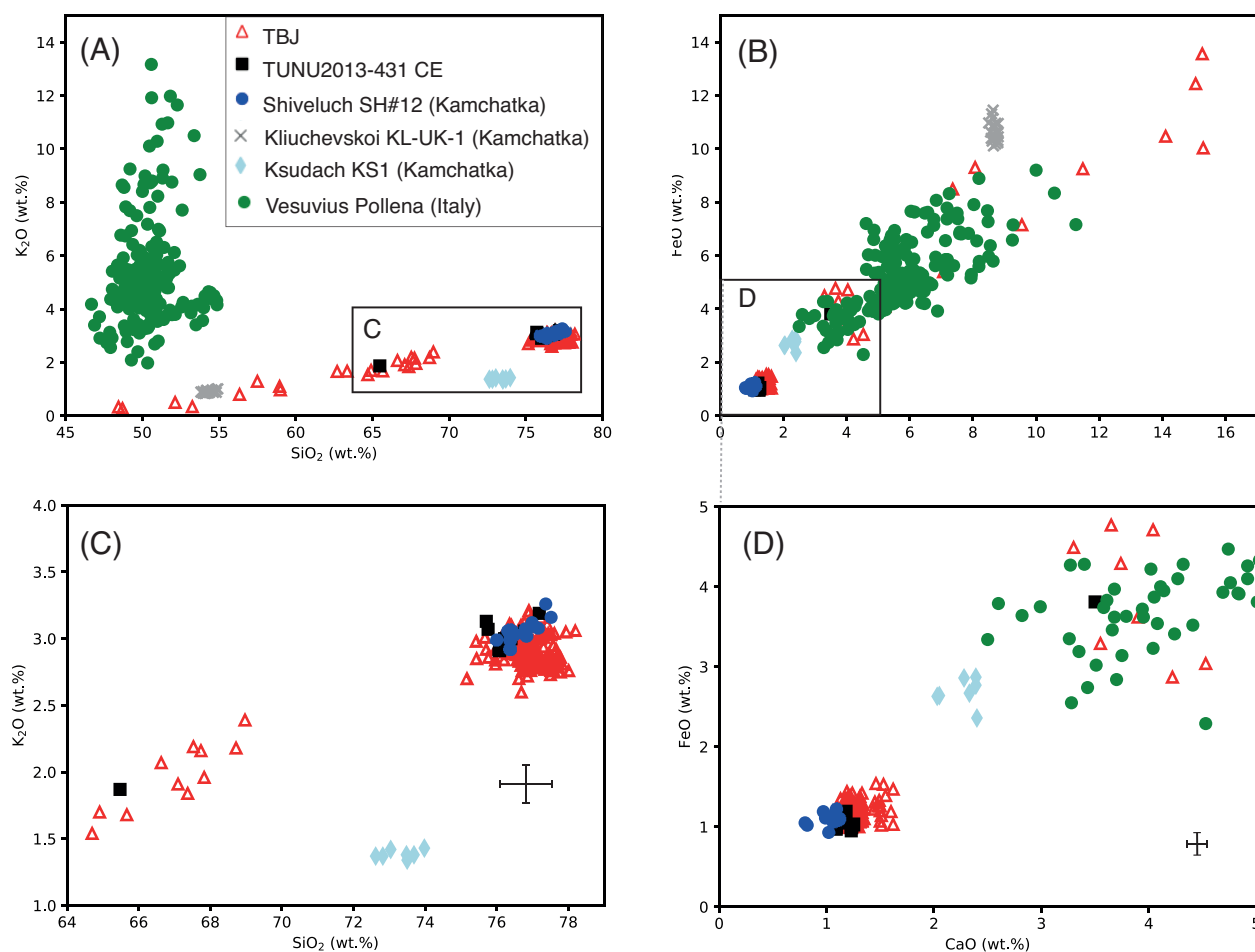


**Figure S6.** Glass major elements geochemical data from the TBJ deposits (red triangles; data from ref. 15), glass shards from the TUNU2013 ice core located at a depth that corresponds to  $431 \pm 2$  CE (black squares), and other known Northern Hemisphere eruptions that occurred around the same time: KS1 eruption of Ksudach (245-360 CE), KL-UK-1 eruption of Kliuchevskoi (325-611 CE), and SH#12 eruption of Shiveluch (542-639 CE) in Kamchatka, Russia (14); and the 472 CE Pollena eruption from Vesuvius, Italy (13). The Shiveluch SH#12 glasses do not display the full compositional range shown in the ice core sample, which is also observed in the TBJ deposits. The error bars ( $\pm 1\sigma$ ) in (C) and (D) are determined from repeat analyses on reference glasses (see the *SI Appendix* SID1 dataset).

### Volatile content of the TBJ magma

The volatile contents of TBJ melt inclusions and matrix glass were analyzed using a JEOL 8600 wavelength dispersive electron microprobe at the University of Oxford. A 15kV, 30 nA defocused (10 micron) beam was used, and each element (F, Cl, P and S) was analyzed simultaneously on one of the 4 wavelength dispersive spectrometers for 120 s (on peak) with background counts collected for half the time on either side of the peak. See the *SI Appendix* dataset (SID1) for the measurements. All S in the melt is presented as  $\text{SO}_2$ .

In an attempt to assess the amount of  $\text{SO}_2$  that was initially dissolved in the TBJ magma and released during the eruption, we analyzed the  $\text{SO}_2$  in the melt that was trapped during the crystallization of the phases. The melt inclusions (MI;  $n=27$ ) and matrix glasses ( $n=92$ ; including re-entrants in crystals) were analyzed from samples through the eruption sequence (Fig. S7). The MI are rare and typically very small (few tens of microns) and found within a variety of crystal phases. The  $\text{SO}_2$  in the

MI ranges from below the detection limit (65 ppm) to 2104 ppm with an average of 442 ppm ( $n=15$ ). The maximum  $\text{SO}_2$  concentration in the matrix glasses is 2051 ppm and the average is 243 ppm ( $n=88$ ). Given these wide and overlapping ranges it was not possible to estimate the amount of sulfur released with any certainty.

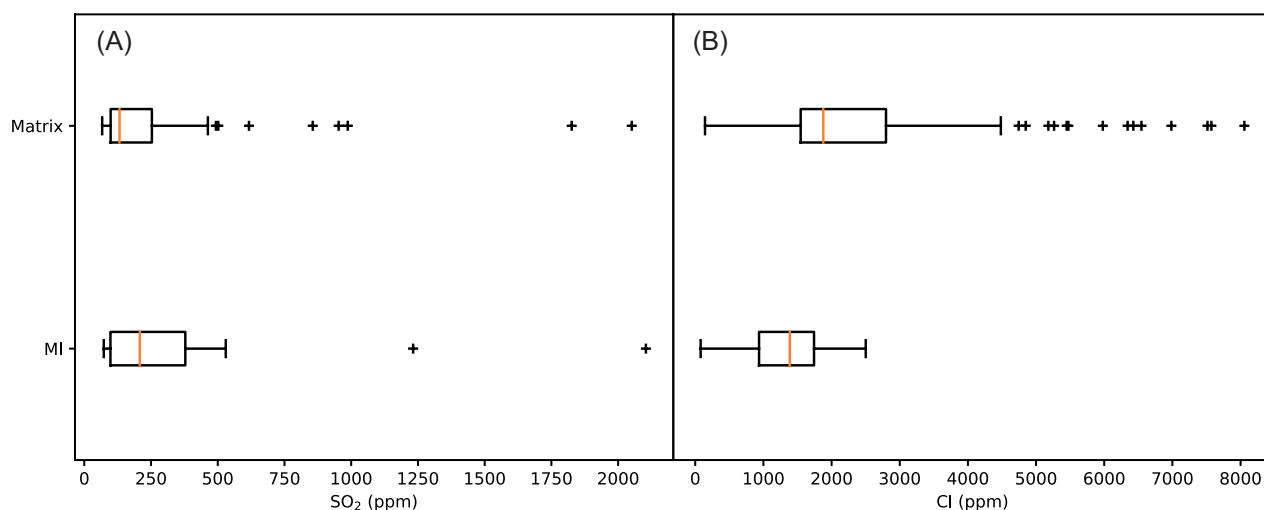


**Figure S7.** Volatile element compositions of melt inclusions trapped within crystals and the matrix glass. (A) The sulfur concentrations in the MI and matrix glasses span a wide range. (B) The matrix glasses have more Cl than the melt inclusions implying the melt was not saturated in Cl.

The fluorine values in the melt are mostly below detection limit ( $<330$  ppm) in both MI and matrix glasses indicating that the F release is likely to have been less than a few Tg (using equation in ref. 16). The chlorine concentrations in the MI are significantly less (avg. 1329 ppm;  $n=23$ ) than those in the matrix glasses (avg. 2423 ppm;  $n=111$ ; Fig. S7). These compositions imply that the melt was not saturated in Cl even though the magma contains apatite with appreciable amounts of Cl (1.7 wt%).

These wide variations in both sulfur and chlorine are most likely associated with late-stage volatile transfer from another magma. Mingled clasts are observed in the deposits indicating that the dominant silicic magma interacted with a basaltic melt during the eruption (15). It is possible that there were significant volumes of S and Cl gas released during the TBJ but our data do not provide reliable constraints.

## References

1. I. Aida, Reliability of a tsunami source model derived from fault parameters. *J Phys Earth* **26**, 57–73 (1978).
2. T. Suzuki, “A theoretical model for dispersion of tephra” in *Arc Volcanism: Physics and Tectonics*, D. Shimozuru, I. Yokoyama, Eds (Tokyo: Terra Scientific Publishing, 1983), pp. 95–116.
3. A. Costa, J.Y. Suzuki, T. Koyaguchi, Understanding the plume dynamics of explosive super-eruptions. *Nat Commun* **9**, 654 (2018).
4. T. Pfeiffer, A. Costa, G. Macedonio, A model for the numerical simulation of tephra fall deposits. *J Volcanol Geotherm Res* **140**, 273–294 (2005).
5. P. Sheets, “Introduction” in *Archaeology and Volcanism in Central America*, P. D. Sheets, Eds (University of Texas Press, 1983), pp. 1-13.
6. R.A. Dull, J.R. Southon, P. Sheets, Volcanism, Ecology and Culture: A Reassessment of the Volcán Ilopango TBJ Eruption in the Southern Maya Realm. *Lat Am Antiq* **12**, 25-44 (2001).

7. P.J. Mehringer, A.M. Sarna-Wojcicki, L.K. Wollwage, P. Sheets, Age and extent of the Ilopango TBJ Tephra inferred from a Holocene chronostratigraphic reference section, Lago De Yojoa, Honduras. *Quat Res* **63**, 199-205 (2005).
8. J.C. Lohse *et al.*, Late Holocene volcanic activity and environmental change in Highland Guatemala. *Quat Sci Rev* **191**, 378-392 (2018).
9. Q. Hua, M. Barbetti, A.Z. Rakowski, Atmospheric Radiocarbon for the Period 1950-2010. *Radiocarbon* **55**, 2059–2072 (2013).
10. R. A. Dull *et al.*, Radiocarbon and geologic evidence reveal Ilopango volcano as source of the colossal 'mystery' eruption of 539/40 CE. *Quat Sci Rev* **222**, 105855 (2019).
11. P.J. Reimer *et al.*, IntCal13 and Marine13 Radiocarbon Age Calibration Curves 0–50,000 Years cal BP. *Radiocarbon* **55**, 1869–1887 (2013).
12. C. Bronk Ramsey, Methods for Summarizing Radiocarbon Datasets. *Radiocarbon* **59**, 1809-1833 (2017).
13. R. Santacroce *et al.*, Age and whole rock-glass compositions of proximal pyroclastics from the major explosive eruptions of Somma-Vesuvius: A review as a tool for distal tephrostratigraphy. *J Volcanol Geotherm Res* **177**, 1–18 (2008).
14. V. Ponomareva *et al.*, A full holocene tephrochronology for the Kamchatka Peninsula region: Applications from Kamchatka to North America. *Quat Sci Rev* **168**, 101–122 (2017).
15. D. Pedrazzi, *et al.*, The Ilopango Tierra Blanca Joven (TBJ) eruption, El Salvador: Volcano-stratigraphy and physical characterization of the major Holocene event of Central America. *J Volcanol Geoth Res* **377**, 1–22 (2019).
16. S. Self, The effects and consequences of very large explosive volcanic eruptions. *Philos Trans R Soc Lond A* **364**, 2073–2097 (2006).
17. S.C. Kuehn *et al.*, The INTAV intercomparison of electron-beam microanalysis of glass by tephrochronology laboratories: Results and recommendations. *Quat Int* **246**, 19–47 (2011).